Published in final edited form as:
Brain. 2008 April ; 131(Pt 4): 928–937. doi:10.1093/brain/awn006.

High-frequency oscillations in human temporal lobe: simultaneous microwire and clinical macroelectrode recordings

Greg A. Worrell[1], **Andrew B. Gardner**[3], **S. Matt Stead**[1,2], **Sanqing Hu**[1], **Steve Goerss**[4], **Gregory J. Cascino**[1], **Fredric B. Meyer**[4], **Richard Marsh**[4], and **Brian Litt**[3]

[1]Department of Neurology, Division of Epilepsy and Electroencephalography, Mayo Clinic, Rochester, MN 55905

[2]Department of Neurology, Division of Child Neurology, Mayo Clinic, Rochester, MN 55905

[3]Departments of Neurology and Bioengineering, University of Pennsylvania, Philadelphia, PA 19104

[4]Department of Neurosurgery, Mayo Clinic, Rochester, MN 55905, USA

Abstract

Neuronal oscillations span a wide range of spatial and temporal scales that extend beyond traditional clinical EEG. Recent research suggests that high-frequency oscillations (HFO), in the ripple (80–250Hz) and fast ripple (250–1000Hz) frequency range, may be signatures of epileptogenic brain and involved in the generation of seizures. However, most research investigating HFO in humans comes from microwire recordings, whose relationship to standard clinical intracranial EEG (iEEG) has not been explored. In this study iEEG recordings (DC − 9000Hz) were obtained from human medial temporal lobe using custom depth electrodes containing both microwires and clinical macroelectrodes. Ripple and fast-ripple HFO recorded from both microwires and clinical macroelectrodes were increased in seizure generating brain regions compared to control regions. The distribution of HFO frequencies recorded from the macroelectrodes was concentrated in the ripple frequency range, compared to a broad distribution of HFO frequencies recorded from microwires. The average frequency of ripple HFO recorded from macroelectrodes was lower than that recorded from microwires (143.3 ± 49.3 Hz versus 116.3 ± 38.4, Wilcoxon rank sum $P<0.0001$). Fast-ripple HFO were most often recorded on a single microwire, supporting the hypothesis that fast-ripple HFO are primarily generated by highly localized, sub-millimeter scale neuronal assemblies that are most effectively sampled by microwire electrodes. Future research will address the clinical utility of these recordings for localizing epileptogenic networks and understanding seizure generation.

Keywords

high-frequency oscillations; ripple; fast ripple; intracranial EEG; epilepsy

Introduction

Two distinct populations of interictal high-frequency oscillations (HFO) called ripples (>80–250 Hz) and fast ripples (FR >250–500 Hz) have been reported in human medial temporal lobe (Bragin *et al.*, 2002*a*). Microwire recordings from the hippocampus of freely behaving rats support an important physiological role for ripple frequency oscillations in memory (Buzsaki,

Correspondence to: G. A. Worrell, Department of Neurology, 200 First St. SW, Rochester, MN 55901, USA, E-mail: worrell.gregory@mayo.edu.

1989; Buzsaki *et al.*, 1992; Buzsaki, 1996, 1998; Behrens *et al.*, 2005; Clemens *et al.*, 2007) and a potential pathological role in the genesis of seizures (Timofeev and Steriade, 2004). In contrast, HFO in the FR range are thought to be uniquely pathological oscillations, and primarily identified in epileptogenic (seizure generating) hippocampus (Bragin *et al.*, 1999*a*, *b*, 2002*a*, 2004; Le Van Quyen *et al.*, 2006). Similar to the studies in rats, microwire recordings from human medial temporal lobe demonstrated ripple frequency oscillations in both epileptogenic and non-epileptogenic hippocampus, but FR oscillations were primarily identified in epileptogenic hippocampus (Bragin *et al.*, 2002*b*). These studies from non-primates and humans support the hypothesis that HFO, and in particular FR oscillations, are important electrophysiological signatures of epileptogenic brain and involved in seizure generation.

Clinical iEEG is typically recorded over a narrow frequency bandwidth (~0.1–100 Hz) from large surface area (~1–10mm^2), widely spaced (5–10 mm) macroelectrodes. Recent studies using broadband iEEG recorded from clinical macroelectrodes have primarily investigated changes in the power spectral density (PSD) over the gamma, ripple and FR frequency bands in association with interictal spikes and at seizure onset (Allen *et al.*, 1992; Fisher *et al.*, 1992; Worrell *et al.*, 2004; Jirsch *et al.*, 2006; Urrestarazu *et al.*, 2007). These studies using subdural and depth macroelectrodes report an increase in broadband high-frequency PSD at seizure onset compared to baseline records, as well as distinct and sustained HFO in the gamma, ripple, and in some cases even FR frequency range (Allen *et al.*, 1992; Fisher *et al.*, 1992; Traub *et al.*, 2001; Worrell *et al.*, 2004; Jirsch *et al.*, 2006). However, changes in high-frequency power may be primarily related to changes in broadband high-frequency activity, and the relation to distinct HFO identified from microwire recordings is unclear. Thus, despite the potential physiological importance of HFO to seizure generation, the connection between microwire (~$10^{-3}mm^2$) and clinical macroelectrode recordings has not been investigated.

In-vivo microwire recordings in rats demonstrate spatially coherent ripple frequency oscillations over the longitudinal extent (~4 mm) of the dorsal CA1 region, and less coherent ripples over the hippocampal–entorhinal pathway (Chrobak and Buzsaki, 1996). In contrast, FR oscillations are spatially localized with the volume of generation estimated to be less than $1mm^3$ (Bragin *et al.*, 2002*a*). This suggests that discrete ripple oscillations, and possibly even FR oscillations, may extend over spatial scales effectively recorded by clinical macroelectrodes that have ~10^3 times the surface area of microwire electrodes. In this paper we describe interictal FR and ripple HFO recorded simultaneously from hybrid depth electrodes containing microwire and clinical macroelectrodes, and investigate their association with epileptogenic brain.

Patients and Methods

Patients

Seven consecutive patients with medically intractable temporal lobe partial epilepsy undergoing evaluation for epilepsy surgery had hybrid depth electrodes (Fig. 1) composed of microwires and clinical macroelectrodes (Adtech Inc.) implanted in the medial temporal lobe structures (amygdalohippocampus). All patients gave their informed consent for participation in the Mayo Clinic Internal Review Broad approved study. These patients underwent depth electrode implantation because standard non-invasive studies were not able to adequately localize a region of seizure onset. All patients were initially presented at a multidisciplinary epilepsy surgery conference, and the consensus clinical opinion was for the patient to have iEEG monitoring to record their habitual seizures in an attempt to better localize the seizure onset zone. Each patient underwent implantation of intracranial depth electrodes according to standard presurgical evaluation protocols (Engel and Pedley, 1997).

Electrodes

Custom hybrid depth electrode designs (AD-Tech Medical Instrument Corporation, Racine, WI) were based on standard four and eight contact clinical depth electrodes. The depth electrodes (Fig. 1) consist of a 1.3 mm diameter polyurethane shaft with Platinum/Iridium (Pt/Ir) clinical macroelectrode contacts; each clinical contact is 2.3 mm long with either a 5 or 10 mm center-to-center spacing (surface area 9.4 mm^2 and impedance ~200–500Ω). In addition to the standard clinical contacts the 8 contact depth has 9 microwires, and the 4 contact depth has 18 microwires, oriented radially along the shaft of the depth (Fig. 1). Each depth has a bundle of 9 Pt/Ir microwires that protrude 1–3 mm from the shaft tip (Bragin *et al.*, 2002*b*). The microwires are made of insulated Pt/Ir wire (40 μm diameter and impedance 500–1000 × 10^3Ω).

Electrode localization

Custom hybrid depth electrodes were stereotactically placed into the medial temporal lobe structures (Amygdala and Hippocampus) using an occipital or lateral approach (Fig. 1). All patients underwent high-resolution 1.5 or 3 Tesla T_1 weighted volumetric MRI brain scans prior to electrode implantation (Jack, 1996), and high-resolution 64-slice CT head scans immediately after electrode implantation. The MRI and CT images were fused and fit to the Talairach brain atlas (Analyze Inc). Electrodes were identified within the fused volume, yielding Talairach coordinates and anatomic structure (e.g. Amygdala and Hippocampus) for each clinical depth electrode. The location of microwire electrodes was inferred from their known relationship to clinical macroelectrodes (Fig. 1). After implantation the patients were admitted to the Epilepsy Monitoring Unit for continuous iEEG monitoring to record their habitual seizures.

Data acquisition

Continuous broadband iEEG was recorded simultaneously from both clinical macroelectrodes and microwires (Neuralynx Inc.: DC capable amplifier, 9000 Hz low-pass filter and sampling at 32 kHz). The unfiltered iEEG from microwire and clinical macroelectrodes was directly archived to a 20 TB RAID for off-line analysis. Subsequently the archived data were low pass filtered and decimated to 5 kHz. The clinical data was acquired from the macroelectrodes with a 128-channel clinical acquisition system (XLTEK Inc.: high-pass filter 0.1 Hz, low-pass filter 100 Hz and sampling at 512 Hz) operating in parallel with the Neuralynx. All clinical decisions were based on the XLTEK recordings and all results reported here were from the Neuralynx recordings.

Scalp, reference and ground electrodes

A limited montage of scalp electrodes were placed according to the 10–20 system (Fp1, Fp2, Fpz, C3, C4). Chin and anterior tibialis EMG signals were obtained for staging sleep. Scalp vertex reference and ground suture electrodes (Ethicon Inc. stainless steel suture) were used for the clinical macroelectrodes. The reference for the microwire recordings was selected from the nine microwires exiting the tip of the depth electrode. The choice of microwire reference was made to minimize noise and artifacts.

Localization of seizure onset zone

For each patient all recorded seizures were visually identified and reviewed. The time of the earliest iEEG change and the associated macroelectrode(s) were selected as the electrographic seizure onset time and seizure onset zone (SOZ), respectively. Seizure onset time and SOZ were determined by independent visual identification of a clear electrographic seizure discharge in macroelectrodes recordings, and then looking backward in the record for the earliest definite iEEG change contiguously associated with the seizure.

Behavioural state

Using video scalp EEG the continuous iEEG recording was staged as wake, non-rapid eye movement sleep, or other (Rechtschaffen and Kales, 1968). Because of the strong modulating impact of behavioural state (sleep/wake) on epileptogenic brain and the established increase in HFO during slow-wave sleep (SWS) (Staba *et al.*, 2004), we randomly selected segments of SWS (non-REM stages 3 and 4) for analysis. All selected data segments were from interictal periods occurring at least 2 h away from seizures.

Data analysis

For each patient ($n = 7$) periods of stages 3 and 4 SWS were visually reviewed and segments of artifact-free data were selected for analysis. A total of 30 min of artifact-free SWS data was analysed for each patient. The clinical macroelectrodes within the SOZ were determined as described earlier, and the channels with the greatest number of HFO events from the SOZ and non-seizure onset zone (NSOZ) were selected for analysis. The SOZ microwire was selected from the group of microwires closest to the SOZ by identifying the microwire with greatest number of HFO events. Electrodes from the NSOZ were selected from regions where macroelectrodes were not involved at seizure onset. Table 1 lists the electrode type, brain location, seizure onset zone, non-seizure onset zone, MRI results and clinical outcome for each patient.

Automated detection of HFO

We utilized an automated detection tool based on the signal line-length measure to screen the data for candidate HFO events (Gardner *et al.*, 2007). Candidate HFO events were subsequently visually reviewed while blinded to the electrode locations, seizure onset zone location and all clinical information. To compensate for the significant spectral roll-off in iEEG over the HFO frequency range (80–1000 Hz) we used first-order backward differencing to effectively equalize the spectral power across the entire HFO frequency range (Shiro and Itzhak, 1982). Detection of HFO events was then achieved by calculating the windowed line-length, and thresholding the magnitude of the line-length segment compared to background. Here the line-length is defined as

$$E^*(t) = \sum_{k=t-N+1}^{t} |V(k) - V(k-1)| \tag{1}$$

where V(t) is the iEEG signal at discrete time t within a window of size N. The line length $E^*(t)$ has the advantage of weighting both the signal amplitude and frequency similarly. For these experiments the line-length is calculated from the band-pass filtered iEGG signal (80–1000 Hz) (Esteller *et al.*, 2001). The line-length statistic produces fewer false positive detections from spikes and large amplitude artifacts compared to simply using high-frequency band-pass energy (Gardner *et al.*, 2007). Lastly, we selected a non-parametric threshold by examining the empirical cumulative distribution function (cdf) of line-length values from a small training set (not included in further analysis), and noting that thresholds corresponding to the 95–98 percentile of the cdf appeared to be good breakpoints for discriminating HFO events from background activity. In this work we deliberately selected a lower threshold (95 percentile) to produce a hypersensitive detector (high sensitivity, low specificity). Processing was performed on an epoch-bases (3 min, non-overlapping segments of data), which resulted in epoch-specific (e.g. data dependent) threshold values. In this manner the threshold was allowed to adapt to background EEG changes. For the current application a large number of false positive detections were generated (~80% of candidate events were false positives), but these were rapidly screened and discarded by expert visual review.

Human verification of HFO

We used a custom MATLAB graphical user interface to present 0.4-s screens of single-channel iEEG (1–1000 Hz) and its high-pass filtered counterpart (80–1000 Hz) for visual identification of HFO. The display gain was calibrated to 10 μV/mm for all signals reviewed. The visual verification task was performed by reviewers blinded to electrode type, seizure onset location or clinical information, and the event automatically saved to a database for future analysis. Each automated detection was reviewed and selected only if there was a distinct HFO of six cycles or greater.

Statistical analysis

Kruskal–Wallis analysis of variance was used to test for any statistically significant difference in the number of HFO events (ripple and fast ripples) recorded from electrode types (macroelectrode and microwire electrodes) and brain regions of interest (SOZ and non-SOZ). *Post hoc* analysis between groups was performed using the Wilcoxon rank sum.

HFO frequency distribution

Histograms of all interictal HFO versus frequency for clinical macroelectrode and microwire were generated, and the average HFO frequencies in the ripple frequency range were examined using Wilcoxon rank sum. All data and statistical analysis performed with MATLAB (MathWorks Inc., Natick, MA).

Results

Localization of seizure onset zone

All seven patients had medial temporal lobe epilepsy as demonstrated by seizure onset from medial temporal lobe depth electrodes. The clinical macroelectrodes associated with the earliest EEG change at seizure onset and their anatomic locations are shown in Table 1. Three patients had seizures originating independently from both the left and right medial temporal lobes, and all seven patients had seizures that originated from the primary SOZ and subsequently propagated to the contralateral medial temporal lobe.

HFO detection, characterization and statistical analysis

Figure 2 and Figure 3 show examples of simultaneous macro and microelectrode recordings. A total of 5569 HFO events were detected from the seven patients, and 843 were subsequently verified after visual review, with 74% (620/843) of the HFO events detected from microwires compared to 26% (223/843) from the clinical macroelectrode. The majority of HFO events, 84% (710/843), were associated with epileptiform sharp waves (Fig. 2 and Fig. 3) (Buzsaki *et al.*, 1992;Bragin *et al.*, 2002*b*;Urrestarazu *et al.*, 2007). The timing of the ripple and FR oscillations was associated with the epileptiform sharp wave, and not the after-coming slow-wave (Fig. 3). In Fig. 4A and Table 2 the total number of microwire and macroelectrode HFO events in SOZ versus non-SOZ are shown for each patient ($n = 7$). Patient #4 had only seven HFO events recorded from all electrodes, but the remaining six patients had greater than 50 HFO events over the 30 min of iEEG analysed. The total number of HFO, ripple and FR events, from microwires for these six patients, excluding patient #4, ranged from (223 to 33 HFO/30 min) in the SOZ compared to (26 to 3 HFO/30 min) in the non-SOZ region. The number of HFO recorded from the clinical macroelectrodes ranged from 52 to 18 (HFO/30 min) in the SOZ to 18 to 3 (HFO/30 min) in the non-SOZ (Table 2).

HFO events, as displayed in Fig. 4B, exhibited a range of spectral characteristics with significant signal complexity. Spectral chirps commonly characterized HFO events (high-frequency onset followed by a shift to lower frequencies, Schiff *et al.*, 2000). The automated

detection and subsequent blinded visual verification yielded distinct HFO that were most often, 83.0% (700/843) of all HFO events detected, localized to one microwire, and the remainder to two adjacent microwires (1mm separation) or a single clinical macroelectrode.

Histograms of the HFO events (microwire and clinical macroelectrodes) sorted by HFO frequency show a primary peak in the number of HFO events in the ripple frequency range for both microwires and clinical macroelectrodes (Fig. 5). The HFO histograms (Fig. 5), however are qualitatively different for microwires and clinical macroelectrodes. The distribution of HFO frequencies recorded with clinical macroelectrodes declines rapidly over the ripple frequency band, and only rare fast-ripple events (>250 Hz) were recorded. In contrast, the distribution of HFO events recorded with microwires shows a broad range of HFO frequencies spanning the ripple and fast-ripple frequency range (80–750 Hz). The wider distribution of HFO frequencies recorded from the microwires yields a higher average HFO ripple (80–250 Hz) frequency compared to macro-electrode ripples, (143.3±49.3 Hz versus 116.3±38.4, Wilcoxon rank sum $P<0.0001$).

Kruskal–Wallis analysis of variance and *post hoc* Wilcoxon rank sum analysis (Fig. 6) were performed to identify differences in group variables of interest: HFO type (ripple/fast ripple), electrode type (macroelectrode/microwire) and brain region (SOZ/non-SOZ). The Kruskal–Wallis analysis demonstrates that the average numbers of HFO are significantly different across all groups (KW statistic = 32.3, $P = 3.5 \times 10^{-5}$), and *post hoc* analysis demonstrates the number of ripple and fast-ripple HFO recorded with both microwire and clinical macroelectrodes were increased in the SOZ compared to the non-SOZ (Fig. 6). In addition, the microwire electrodes detect significantly more fast-ripple HFO compared to the clinical macroelectrodes, $P<0.01$.

Discussion

In this study broadband iEEG was recorded simultaneously from hybrid depth electrodes containing both clinical macroelectrodes and multiple microwires. This approach yields information, albeit coarse grained, over the range of spatial scales reported for interictal HFO in the ripple and FR frequency range (Chrobak and Buzsaki, 1996; Bragin *et al.*, 2002*a*). Of potential clinical relevance is the direct comparison of ripple and FR oscillations recorded from clinical macroelectrodes and microwires.

The results support the hypothesis that the local field potentials recorded by microwires and clinical macroelectrodes are qualitatively different, as evidenced by recordings of HFO with broadband iEEG. We speculate that this is due to the significant difference in electrode surface area (10^{-3}mm^2 versus 9.3 mm^2 for the electrodes used here), and the physical properties of neuronal assemblies generating these activities. The distribution of HFO frequencies recorded with microwires exhibit a continuum spanning the ripple and FR range (Fig. 5). In contrast, the distribution of HFO frequencies recorded with macroelectrodes falls off more rapidly with frequency, and only rare FR HFO are observed (Fig. 5). The number of HFO detected decreases with increasing frequency, and in our data does not clearly show distinct HFO modes in the ripple in FR ranges (Staba *et al.*, 2002*a*). In addition, because the HFO distributions are qualitatively different the population of ripple frequency HFO events recorded from the microwires has significantly higher mean frequency (143.3±49.3 Hz) compared to the macroelectrode (116.3 ± 38.4 Hz), $P<0.0001$. We speculate that the reason for the wider range of HFO frequencies for the microwire recordings, and the markedly reduced occurrence of FR events on the clinical macroelectrode, is related to the spatial extent of the cell assemblies generating HFO events. The effective spatial averaging of local field potentials by the comparatively large surface area of clinical macroelectrodes would then have the effect of spatially undersampling focal HFO activity. This hypothesis is consistent with our results showing highly focal HFO that are most often evident on one or two microwires (spaced 1 mm

apart), and not evident on adjacent macroelectrodes and more distant microelectrodes. These findings are also consistent with the previous reports showing that FR oscillations are localized to regions <1 mm^3 (Bragin *et al.*, 2002*a*). A test of this hypothesis will have to wait for experiments currently underway utilizing microwire arrays with greater spatial sampling to clearly delineate the relationship between oscillation frequency and spatial extent of HFO. In fact, it is not currently possible to rule out that the macroelectrode itself disrupts the generation of FR HFO; possibly by producing an equipotential surface disrupting the generation of FR oscillations.

Similar to previously studies using only microwire recordings (e.g. Bragin *et al.*, 1999*a*, 2002*a*, *b*; Staba *et al.*, 2002*a*, *b*) or only clinical macroelectrodes (Urrestarazu *et al.*, 2007), we identified interictal ripple and FR HFO in epileptogenic mesial temporal lobe (Amygdala, Hippocampus and Entorhinal Cortex). The simultaneous recordings support the hypothesis that HFO (80–1000 Hz), ripple and FR events, are increased in the SOZ compared to non-SOZ for both microwire and clinical macroelectrode recordings (Fig. 6), and that the microwires are superior for detecting FR HFO (Fig. 6). In contrast to the previous reports using only microwire recordings (Staba *et al.*, 2002*a*, 2004), we did not observe a decrease in the number of ripple HFO in the SOZ, but rather found an increase in ripple and FR HFO in the SOZ with both microwires and clinical macroelectrodes. The origin of the difference between our results and previous studies showing decreased ripple HFO in the SOZ is not clear, but may relate to the patients studied. Previous reports using microwires were primarily from patients with hippocampal atrophy on MRI, and were subsequently shown by pathology to have mesial temporal sclerosis (Bragin *et al.*, 1999*a*, 2002*b*; Staba *et al.*, 2002*a*, *b*). In contrast, only two of the patients studied here had MRI evidence of hippocampal atrophy suggestive of mesial temporal sclerosis. Thus our finding that there is an increase in ripple frequency HFO, rather than a decrease as reported previously (Bragin *et al.*, 2002*b*), may reflect the absence of more dramatic structural abnormalities in the patients studied. Our finding is, however, consistent with the other reports from humans and non-primates that show an increase in ripple frequency HFO at, or prior to, the onset of seizures (Grenier *et al.*, 2001; Traub *et al.*, 2001; Dzhala and Staley, 2003; Urrestarazu *et al.*, 2007). In cat neocortex Grenier *et al.* (2001) demonstrate that ripple HFO are strongly associated with the onset of focal seizures, and that pathological ripple HFO may play a fundamental role in the actual generation of seizures. From *in vivo* intracellular recordings they show evidence for ripple oscillations influencing the transmembrane potential of surrounding neurons, which acts to recruit additional neurons into the ripple frequency oscillation. Because the majority of neurons are excitatory, the recruited neurons act to further depolarize adjacent cells, and the action potentials of recruited neurons directly contribute to the local ripple field. They hypothesize that beyond a certain threshold the ripple HFO field potential takes over and produces a pathological recruiting avalanche of high-frequency activity leading to seizure generation. We speculate that such a recruiting feedback mechanism might not always degenerate into a seizure, but rather could simply lead to promoting the occurrence of ripple frequency HFO. Thus, within this hypothesis it is reasonable to anticipate an increase in ripple frequency oscillations, as is observed in our data.

Ultimately, the distinction between pathological and physiological HFO may not be confined to HFO in the FR range. There is evidence to support that ripple and gamma frequency HFO are involved in seizure generation, and are not only normal activity (Grenier *et al.*, 2001; Traub *et al.*, 2001; Dzhala and Staley, 2003; Worrell *et al.*, 2004; Urrestarazu *et al.*, 2007). In the absence of large prospective clinical studies to evaluate the utility of high frequency and microelectrode recording, it is important to note that current clinical intracranial EEG using narrow bandwidth recordings (~0.5–100 Hz) from large, widely spaced clinical macroelectrodes is missing potentially important electrophysiology. A central question that remains to be answered is the optimal temporal and spatial resolution of human intracranial electrophysiology for diagnostic and therapeutic applications.

Acknowledgements

This work was supported by funding from the Epilepsy Research Foundation, CURE foundation, Mayo Clinic Foundation, and the National Institutes of Health grant #K23 NS 4795. Dr. Litt's research is funded by the National Institutes of Health (RO1NS048598, 1NS041811-01), the Klingenstein Foundation, the Dana Foundation, The Epilepsy Project, the Pennsylvania Tobacco Fund, and the Whitaker Foundation. Funding to pay the Open Access publication charges for this article was provided by the Mayo Clinic.

References

Allen PJ, Fish DR, Smith SJ. Very high-frequency rhythmic activity during SEEG suppression in frontal lobe epilepsy. Electroencephalogr Clin Neurophysiol 1992;82:155–159. [PubMed: 1370786]

Behrens CJ, van den Boom LP, de Hoz L, Friedman A, Heinemann U. Induction of sharp wave-ripple complexes in vitro and reorganization of hippocampal networks. Nat Neurosci 2005;8(11):1560–1567. [PubMed: 16222227]

Bragin A, Engel J Jr, Wilson CL, Fried I, Buzsaki G. High-frequency oscillations in human brain. Hippocampus 1999a;9:137–142. [PubMed: 10226774]

Bragin A, Engel J Jr, Wilson CL, Fried I, Mathern GW. Hippocampal and entorhinal cortex high-frequency oscillations (100–500 Hz) in human epileptic brain and in kainic acid-treated rats with chronic seizures. Epilepsia 1999b;40:127–137. [PubMed: 9952257]

Bragin A, Mody I, Wilson CL, Engel J Jr. Local generation of fast ripples in epileptic brain. J Neurosci 2002a;22:2012–2021. [PubMed: 11880532]

Bragin A, Wilson CL, Almajano J, Mody I, Engel J Jr. High-frequency oscillations after status epilepticus: epileptogenesis and seizure genesis. Epilepsia 2004;45:1017–1023. [PubMed: 15329064]

Bragin A, Wilson CL, Staba RJ, Reddick M, Fried I, Engel J Jr. Interictal high-frequency oscillations (80–500 Hz) in the human epileptic brain: entorhinal cortex. Ann Neurol 2002b;52:407–415. [PubMed: 12325068]

Buzsaki G. Two-stage model of memory trace formation: a role for "noisy" brain states. Neuroscience 1989;31:551–570. [PubMed: 2687720]

Buzsaki G. The hippocampo-neocortical dialogue. Cereb Cortex 1996;6:81–92. [PubMed: 8670641]

Buzsaki G. Memory consolidation during sleep: a neurophysiological perspective. J Sleep Res 1998;7:17–23. [PubMed: 9682189]

Buzsaki G, Horvath Z, Urioste R, Hetke J, Wise K. High-frequency network oscillation in hippocampus. Science 1992;256:1025–1027. [PubMed: 1589772]

Chrobak JJ, Buzsaki G. High-frequency oscillations in the output networks of the hippocampal- entorhinal axis of the freely behaving rat. J Neurosci 1996;16:3056–3066. [PubMed: 8622135]

Clemens Z, Molle M, Eross L, Barsi P, Halasz P, Born J. Temporal coupling of parahippocampal ripples, sleep spindles and slow oscillations in humans. Brain 2007;130(Pt 11):2868–2878. [PubMed: 17615093]

Dzhala VI, Staley KJ. Transition from interictal to ictal activity in limbic networks in vitro. J Neurosci 2003;23:7873–7880. [PubMed: 12944517]

Engel, JJ.; Pedley, TA. Epilepsy: a comprehensive textbook. Philadelphia, PA: Lippincott-Raven Publishers; 1997.

Esteller, R.; Echauz, J.; Tcheng, T.; Litt, B.; Pless, B. Line Length: an efficient feature for seizue onset detection; Proceedings of the 23rd Annual International Conference of the IEEE Engineering in Medicine and Biology Society; 2001. p. 1707-1710.

Fisher RS, Webber WR, Lesser RP, Arroyo S, Uematsu S. High-frequency EEG activity at the start of seizures. J Clin Neurophysiol 1992;9:441–448. [PubMed: 1517412]

Gardner A, Worrell G, Marsh E, Dlugos DJ, Litt B. Human and automated detection of high-frequency oscillation in clinical intracranial EEG recordings. J Clin Neurophysiol 2007;118:1134–1143.

Grenier F, Timofeev I, Steriade M. Focal synchronization of ripples (80–200 Hz) in neocortex and their neuronal correlates. J Neurophysiol 2001;86:1884–1898. [PubMed: 11600648]

Jack CR Jr. Magnetic resonance imaging in epilepsy. Mayo Clin Proc 1996;71:695–711. [PubMed: 8656712]

Jirsch JD, Urrestarazu E, LeVan P, Olivier A, Dubeau F, Gotman J. High-frequency oscillations during human focal seizures. Brain 2006;129:1593–1608. [PubMed: 16632553]

Le Van Quyen M, Khalilov I, Ben-Ari Y. The dark side of high-frequency oscillations in the developing brain. Trends Neurosci 2006;29:419–427. [PubMed: 16793147]

Rechtschaffen, A.; Kales, A. A manual for standardized terminology, techniques and scoring system for sleep stages of human subjects. Bethesda, MD: Neurological Information Network; 1968.

Schiff SJ, Colella D, Jacyna GM, Hughes E, Creekmore J, Marshall A, et al. Brain chirps: spectrographic signatures of epileptic seizures. Clin Neurophysiol 2000;111:953–958. [PubMed: 10825700]

Shiro U, Itzhak A. Digital low-pass differentiation for biological signal processing. IEEE Trans Biomed Eng 1982;29:686–693. [PubMed: 6897393]

Staba RJ, Wilson CL, Bragin A, Fried I, Engel J Jr. Quantitative analysis of high-frequency oscillations (80–500 Hz) recorded in human epileptic hippocampus and entorhinal cortex. J Neurophysiol 2002a; 88:1743–1752. [PubMed: 12364503]

Staba RJ, Wilson CL, Bragin A, Fried I, Engel J Jr. Sleep states differentiate single neuron activity recorded from human epileptic hippocampus, entorhinal cortex, and subiculum. J Neurosci 2002b; 22:5694–5704. [PubMed: 12097521]

Staba RJ, Wilson CL, Bragin A, Jhung D, Fried I, Engel J Jr. High-frequency oscillations recorded in human medial temporal lobe during sleep. Ann Neurol 2004;56:108–115. [PubMed: 15236407]

Timofeev I, Steriade M. Neocortical seizures: initiation, development and cessation. Neuroscience 2004;123:299–336. [PubMed: 14698741]

Traub RD, Whittington MA, Buhl EH, LeBeau FE, Bibbig A, Boyd S, et al. A possible role for gap junctions in generation of very fast EEG oscillations preceding the onset of, and perhaps initiating, seizures. Epilepsia 2001;42:153–170. [PubMed: 11240585]

Urrestarazu E, Chander R, Dubeau F, Gotman J. Interictal high-frequency oscillations (100–500 Hz) in the intracerebral EEG of epileptic patients. Brain 2007;130(Pt 9):2354–2366. [PubMed: 17626037]

Urrestarazu E, Jirsch JD, LeVan P, Hall J, Avoli M, Dubeau F, et al. High-frequency intracerebral EEG activity (100–500 Hz) following interictal spikes. Epilepsia 2006;47:1465–1476. [PubMed: 16981862]

Worrell GA, Parish L, Cranstoun SD, Jonas R, Baltuch G, Litt B. High-frequency oscillations and seizure generation in neocortical epilepsy. Brain 2004;127:1496–1506. [PubMed: 15155522]

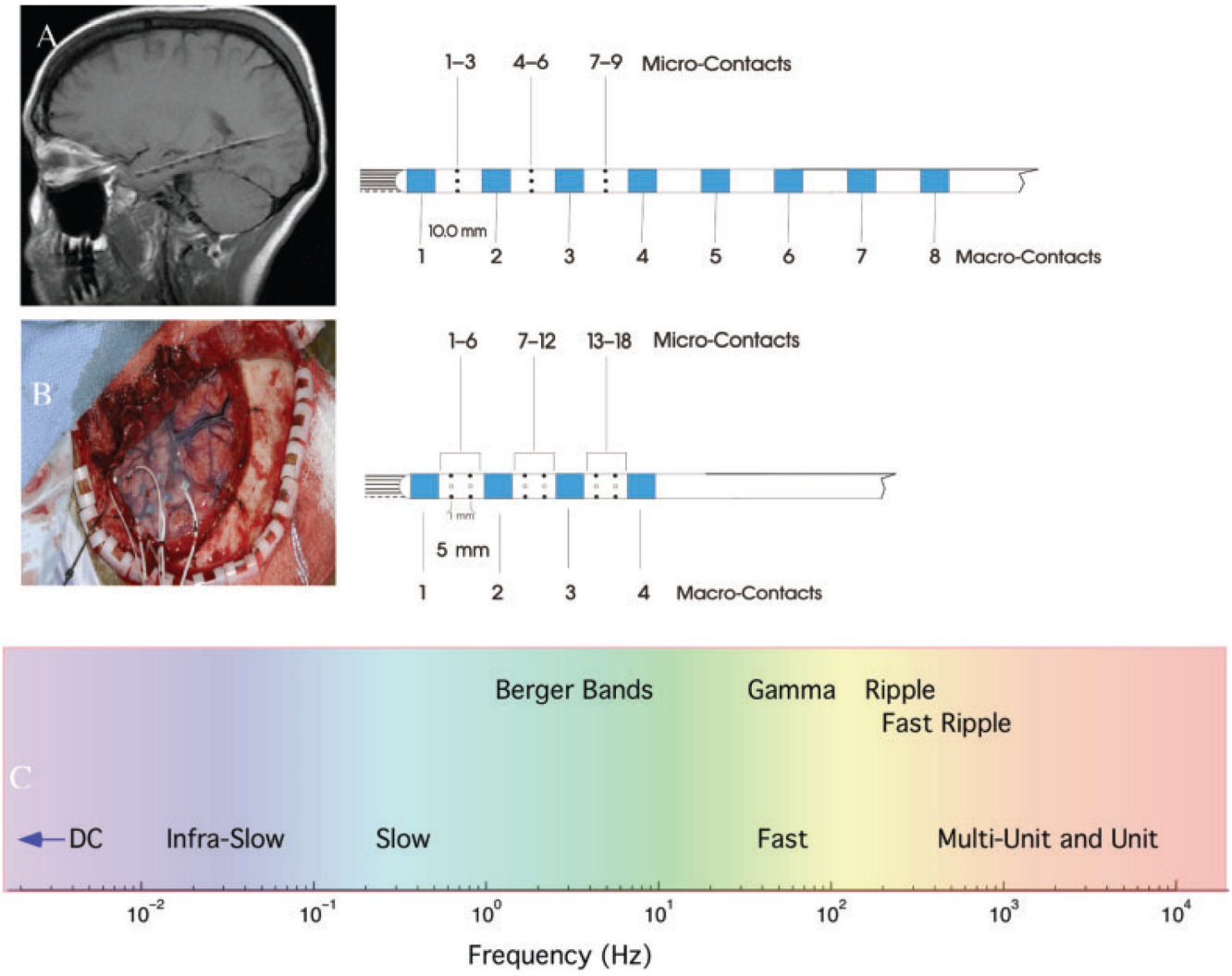

Fig. 1.

(**A**) MRI showing hybrid depth electrode (Adtech, Inc.) implanted along the longitudinal axis of the hippocampus via a posterior burr hole (Patient #1). The hybrid depth electrodes are composed of eight clinical macroelectrodes (blue), nine microwires (black) exiting the tip of the depth and nine radially oriented microwires along the shaft of the depth. The first clinical macrocontact is targeted at the amygdala. (**B**) Left temporal craniotomy (Patient #3) showing a 4× 6 subdural grid over temporal neocortex and hybrid depth electrodes placed through the grid into mesial temporal structures. The hybrid depth electrodes used for lateral approach are composed of 4 clinical macroelectrodes (blue), 9 microwires (black) exiting the tip of the depth and 18 microwires along the depth shaft. (**C**) Spectrum of human brain activity recorded from the hybrid depth electrodes.

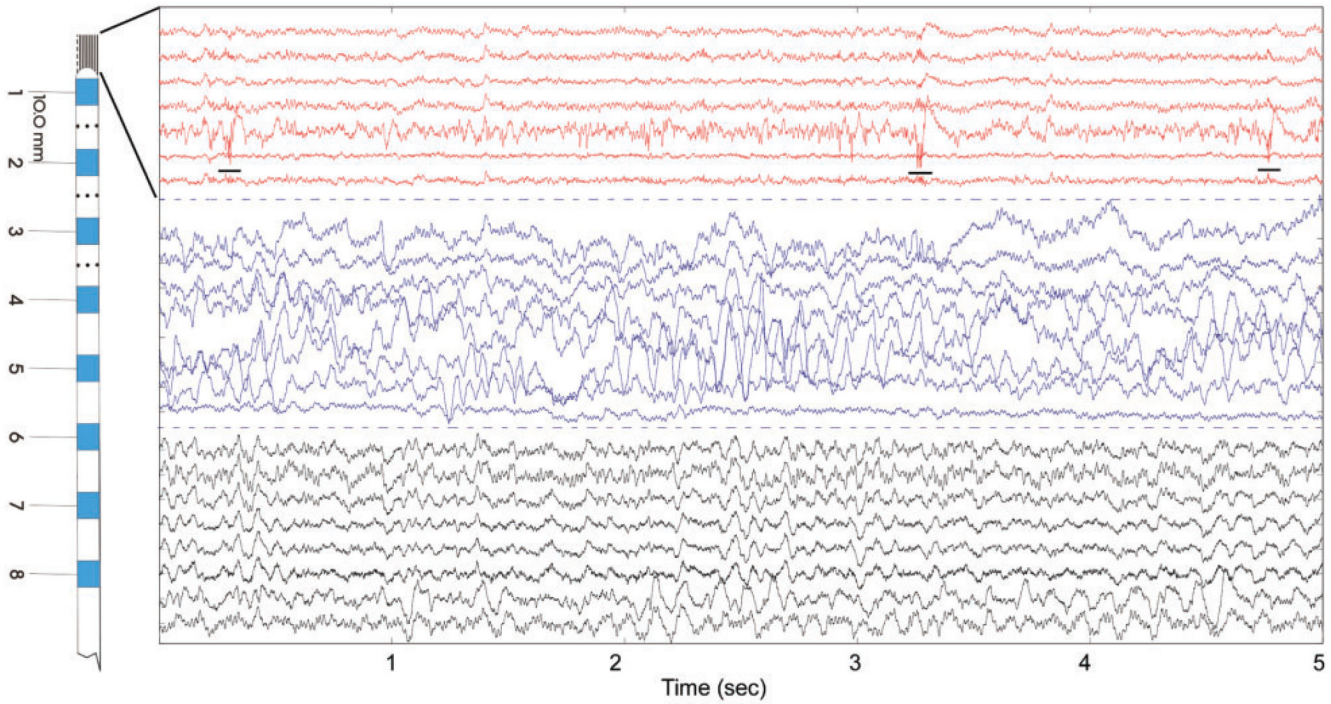

Fig. 2.

Five seconds of raw iEEG (Pt#2) recorded from mesial temporal lobe using eight-contact hybrid depth electrode (Fig. 1A). From the top, channels 1–7 (red) are from a microwire bundle extending from the electrode tip, channels 8–15 are the clinical macroelectrodes (blue) and the channels 16–23 are the shaft microwires. Channels with poor signal omitted from figure. Note fast-ripple oscillations on microwire #5 (underlined) that are not apparent on adjacent microwires or clinical macroelectrode (see also Fig. 3). (Note: microwire channels with significant artifact not shown).

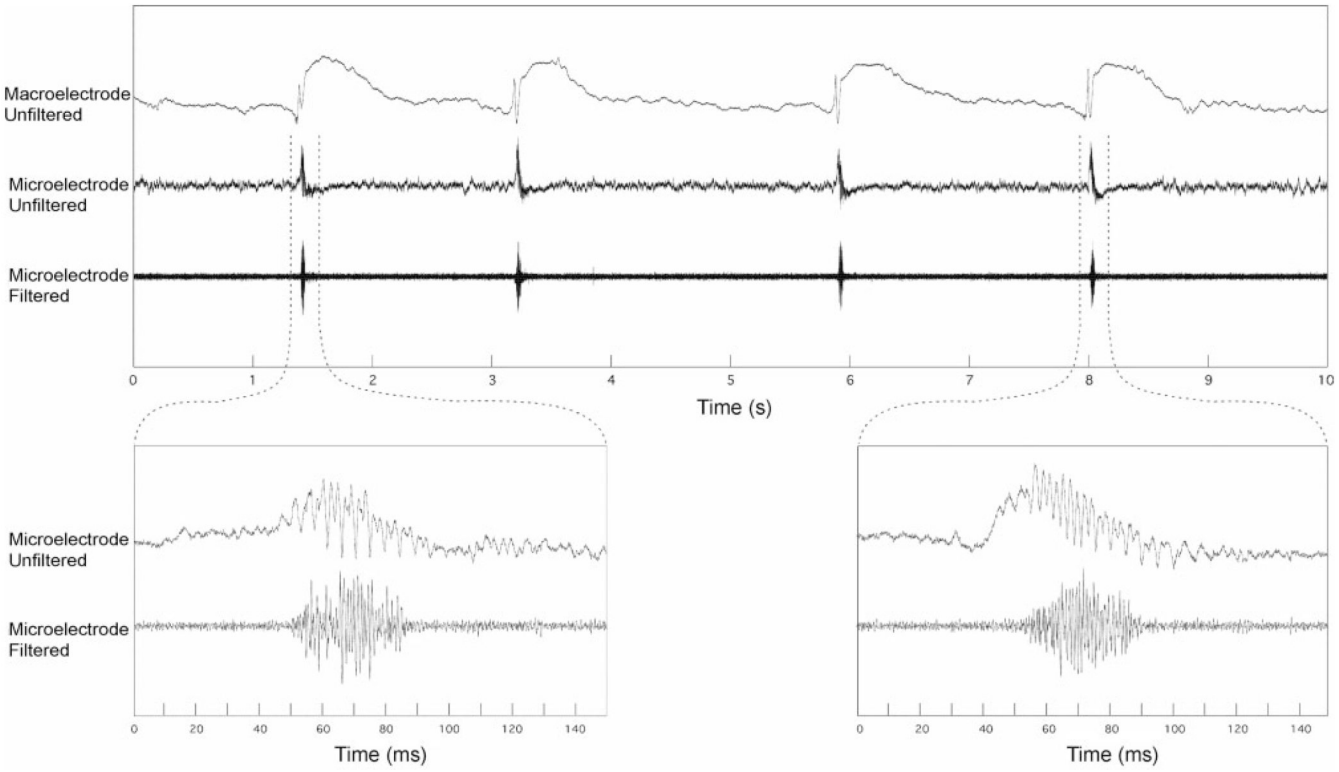

Fig. 3.

(Top panel) Interictal epileptiform spike microwire and adjacent clinical macroelectrodes (Pt #3). The after-coming slow-wave seen on the referential macroelectrode recording is not present on the microwire because of the local recording reference used for microwires. (Lower) Unfiltered and high-pass filtered (>80Hz) microwire recordings highlighting the high-frequency oscillation that is not present on adjacent macroelectrode recording. The high-pass filtered microwire recording (600–6000Hz) shows robust multi-unit activity in association with the fast-ripple oscillation.

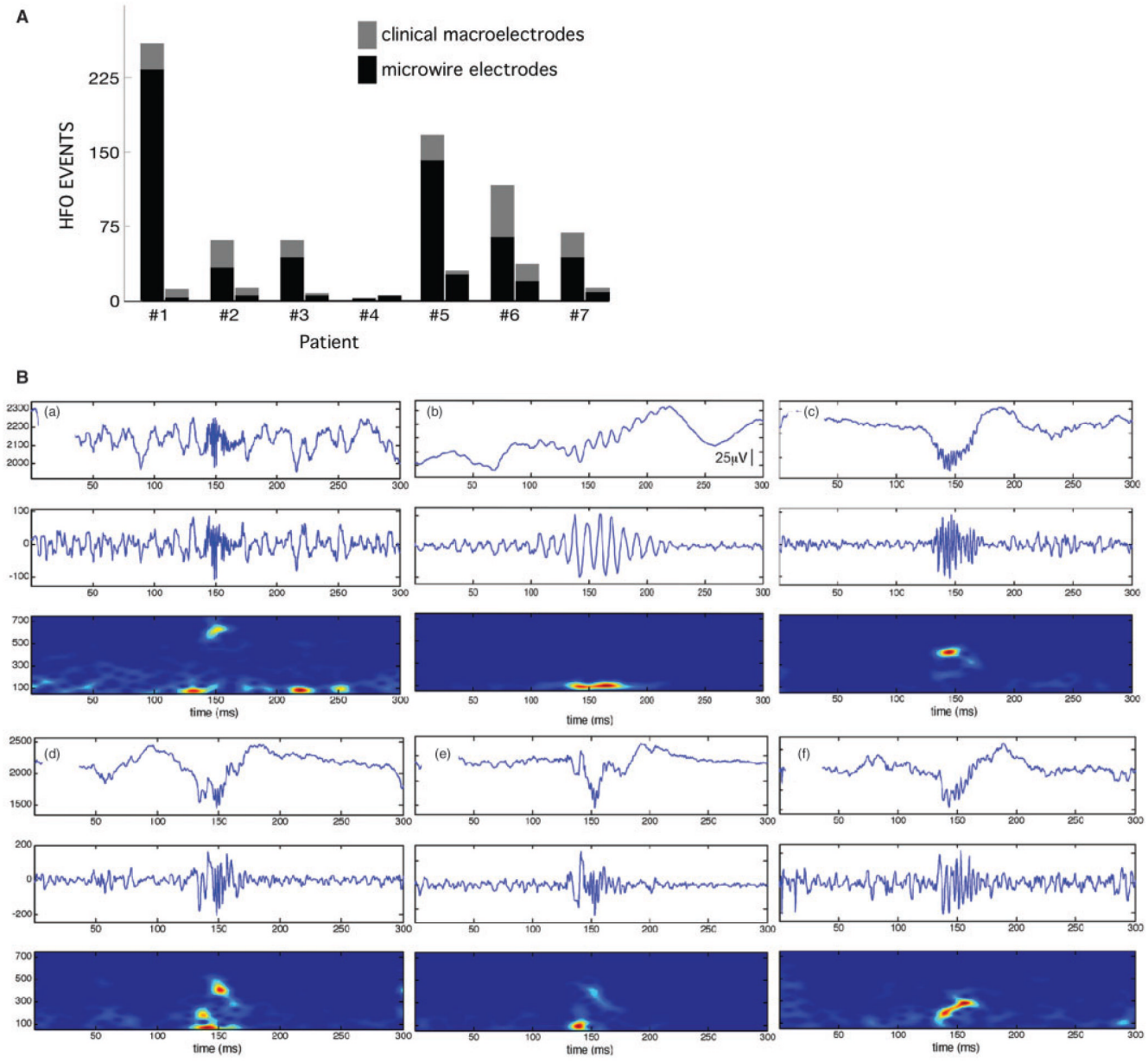

Fig. 4.

(**A**) The total number of verified HFO (ripple and FR) for each patient (n =7) in the SOZ and non-SOZ. (**B**) Representative HFO examples. Each plot shows three views of HFO activity over a 300 ms epoch: (top) unfiltered EEG with an HFO event centred at 150ms, (middle) high-pass filtered EEG (80–1000Hz), (bottom) spectrogram (2.6 ms window). Note that HFOs are primarily characterized by a sharp spectral mode in the FR (a) or ripple frequency range (b). However, many HFOs exhibit more complicated time–frequency structure (c– e), with high-frequency onset followed by slowing of the frequency of the oscillatory event, or conversely ripple frequency at onset that evolved to higher frequency (f). The spectral complexity of these HFEO events highlights the difficulty assigning a single representative frequency.

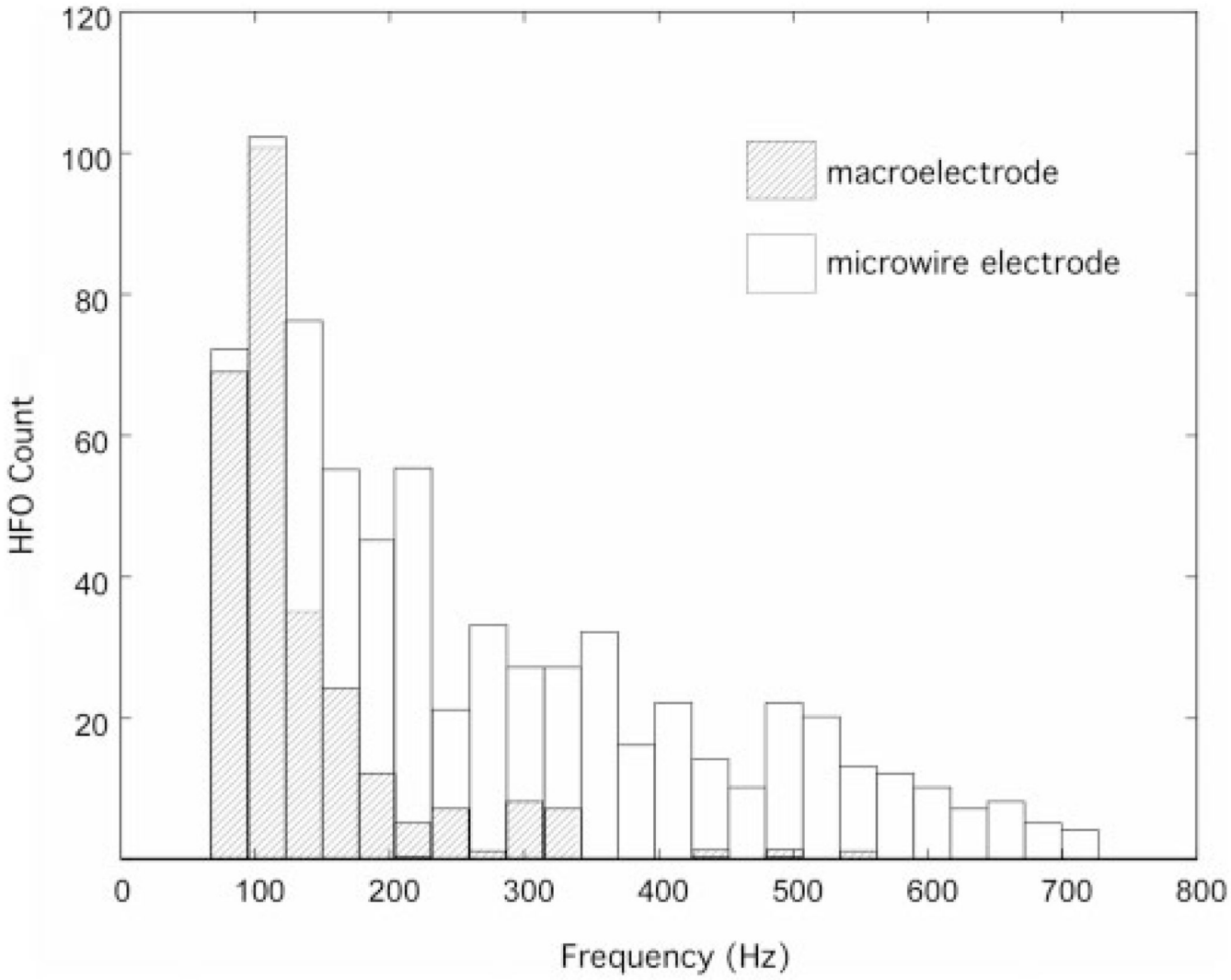

Fig. 5.

Histograms(*n* =7 patients) show the total number of interictal HFO versus frequency recorded from clinical macroelectrodes (hatched) and microwires (open). The distribution of HFO events are qualitatively different for macroelectrode and microwires. The distribution of HFO recorded from the microwires demonstrates a broad continuum of events extending over the ripple and fast-ripple frequency range. In contrast, the distribution of HFO recorded from the clinical macroelectrodes decreases rapidly with frequency, and only rare fast-ripple HFO were recorded. The average ripple frequency (80–250Hz), HFO recorded from microwires was greater than HFO recorded from clinical macroelectrodes (143.3 ± 49.3 Hz versus 116.3 ± 38.4, *P*=0.0001).

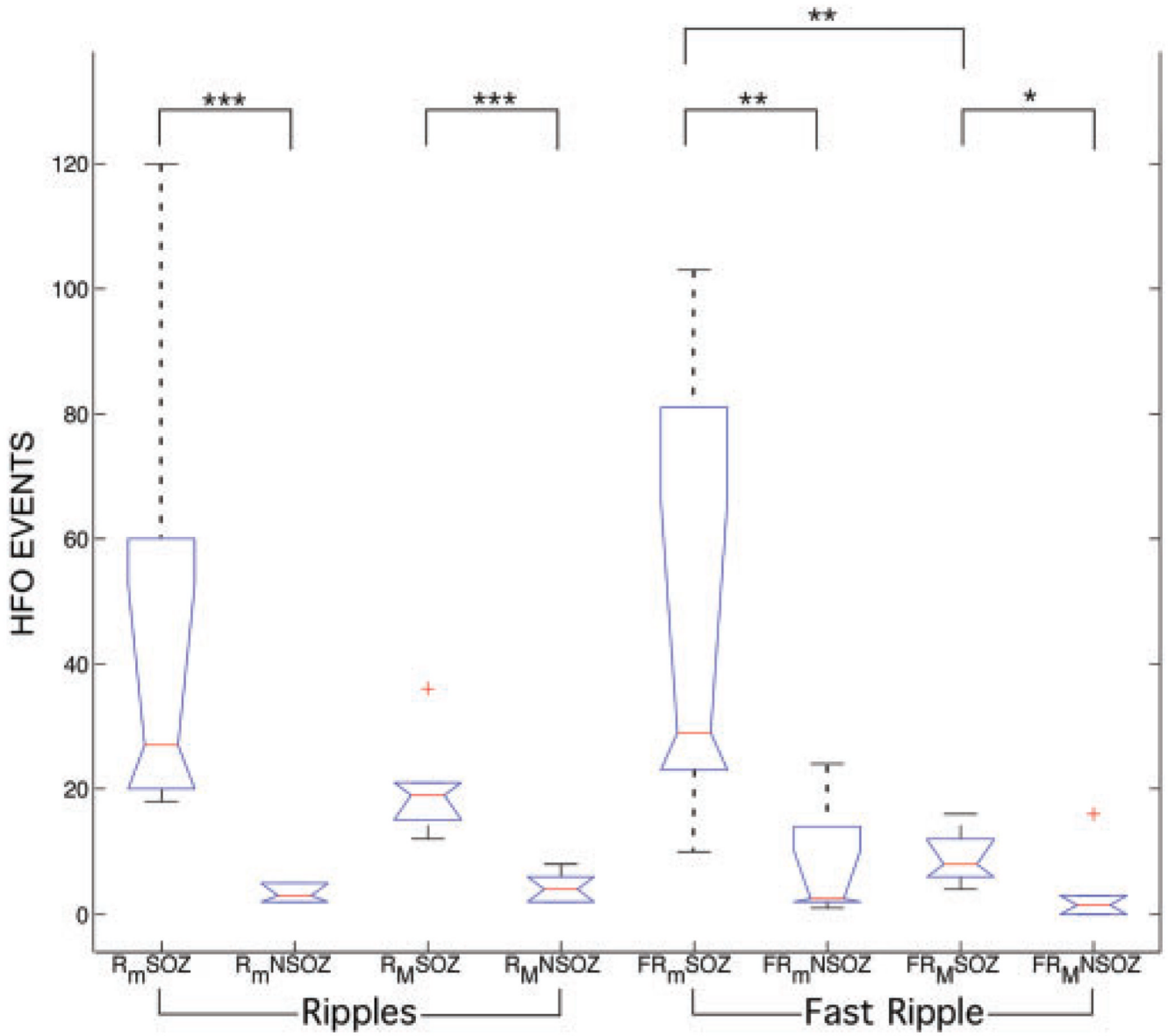

Fig. 6.

Kurskal–Wallis analysis of variance (test statistic=32.34, $P=3.5 \times 10^{-5}$) was applied to three groups of variables: HFO frequency range (ripple/FR), electrode type (microwire/macroelectrode) and brain region of interest (seizure onset/non-seizure onset). Box-plots and the results from *post hoc* analysis using Wilcoxon rank sum (***$P<0.002$, **$P<0.01$, *$P<0.05$) are shown. The lower and upper borders of the box-plots, 25 and 75% percentile of the data, contain the data median indicated by the red line. The whiskers extend over the entire range of the data, and data outliers are indicated by a red cross. The number of microwire ripple (R_m) and fast ripple (FR_m) oscillations are increased in the SOZ compared to non-seizure onset regions (non-SOZ). The number of macroelectrode ripple (R_M) and fast ripple (FR_M) oscillations were increased in the SOZ compared to non-SOZ, but less significance for fast-ripple HFO. The microwire electrodes detect significantly more fast-ripple HFO compared to the clinical macroelectrodes.

Brain. Author manuscript; available in PMC 2009 October 11.

Table 1

Summary of clinical data

Patient	Electrodes	Interictal EEG	SOZ Electrodes (Anatomic location)	Non-SOZ	MRI	Surgery outcome
1	Right and Left Temporal Depths: 8-contact RTD & LTD hybrid	Bitemporal: LTD 1,2,3,4 RTD 1,2	7 Left Temporal Seizures LTD 3,4,5 (AHC) 2 Right temporal Seizures RTD 1,2 (AMD &AHC)	RTD 5	Bilateral HC Atrophy (L≫R)	No Surgery
2	Right and Left Temporal Depths: 8-contact RTD & LTD hybrid	Bitemporal: LTD 1,2 RTD 1,2	6 Right Temporal Seizures RTD 1,2 (AMD) 2 Left Temporal Seizures LTD 2 (AHC)	LTD 5	Bilateral HC Atrophy (L≫R)	No Surgery
3	Left Temporal Grid: 24 contact (4×6) Depths: AD, MD & PD hybrids	Left Temporal: AD 1,2 MD 1,2	2 Left Temporal Seizures AD 1,2 (AMD) MD 1,2 (AHC)	PHC 1	Normal	Left ATL Seizure Free
4	Left Temporal: Grid:36 contact (6×6) Depths: AD, MD & PD hybrids	Left Temporal: AD 1,2	3 Left Temporal Seizures AD 1,2 (AMD) MD 1,2 (AHC)	PD 1	Normal	Left ATL Seizure Free
5	Right and Left Temporal Depths: RTD & LTD hybrids	Left Temporal LTD 1,2	5 Left Temporal Seizures LTD 1,2 (AMD & AHC)	RD 1	Increased T_2 signal Left HC	Left ATL Rare Seizures Engel class II
6	Right and Left Temporal Depths: RTD & LTD hybrids	Bitemporal: LTD 1,2 RTD 1	3 Right Temporal Seizures RTD 1 (AMD)	LTD 1	Normal	Right ATL Seizure Free
7	Right and Left Temporal Depths: RTD & LTD hybrids	Bitemporal: LTD 1,2 RTD 1,2	4 Left Temporal Seizures LTD 1,2 (AMD & AHC) 2 Right temporal Seizures RTD 1,2 (AMD &AHC)	RTD 6	Normal	No Surgery

8-macrocontacts & 18-microwires right temporal depth (RTD) and left temporal depth (LTD) (Figure 1A); 4-macrocontacts & 20 -microwires anterior depth (AD), middle depth (MD), and posterior depth (PD) (Figure 1B); Anterior temporal lobectomy (ATL), Amygdala (AMD), Anterior Hippocampus (AHC), Hippocampus (HC), Entorrhinal cortex (EC), Posterior Hippocampus (PHC).

Table 2

Summary of high frequency oscillation detections

Patient	Total number of HFO (SOZ vs. NSOZ)	Clinical Macroelectrode (SOZ vs. NonSOZ)	Microwire Electrode (SOZ vs. NonSOZ)
1	250 vs. 12	HFO: 27 vs. 9	HFO: 233 vs. 3
		Ripple: 15 vs. 6	Ripple: 120 vs 2
		Fast Ripple: 12 vs. 3	Fast Ripple: 103 vs. 1
2	61 vs 13	HFO: 28 vs. 8	HFO: 33 vs. 5
		Ripple: 18 vs 8	Ripple: 23 vs 3
		Fast Ripple: 10 vs. 0	Fast Ripple: 10 vs. 2
3	61 vs 8	HFO: 18 vs. 3	HFO: 43 vs. 5
		Ripple HFO: 12 vs 3	Ripple: 20 vs. 3
		Fast Ripple HFO: 6 vs. 0	Fast Ripple: 23 vs. 2
4	2 vs 5	HFO: 0 vs. 0	HFO: 2 vs. 5
		Ripple HFO: 0 vs. 0	Ripple: 2 vs. 5
		Fast Ripple HFO: 0 vs. 0	Fast Ripple: 0 vs. 0
5	167 vs. 30	HFO: 26 vs. 4	HFO: 141 vs. 26
		Ripple HFO: 20 vs. 4	Ripple: 60 vs. 2
		Fast Ripple HFO: 6 vs. 0	Fast Ripple: 81 vs. 24
6	116 vs. 37	HFO: 52 vs. 18	HFO: 64 vs. 19
		Ripple HFO: 36 vs. 2	Ripple: 31 vs. 5
		Fast Ripple HFO: 16 vs. 14	Fast Ripple: 33 vs. 14
7	68 vs. 13	HFO: 25 vs. 5	HFO: 43 vs. 8
		Ripple HFO: 21 vs. 2	Ripple: 18 vs. 5
		Fast Ripple HFO: 4 vs. 3	Fast Ripple: 25 vs. 3
Total	725 vs. 118	Total HFO: 176 vs. 47	Total HFO: 549 vs. 71
	843 HFO	Ripple: 122 vs. 25	Ripple: 274 vs. 25
		Fast Ripple: 54 vs. 22	Fast Ripple: 275 vs. 46

High frequency oscillations (HFO);Seizure onset zone(SOZ); Non-Seizure onset zone(NSOZ). All results from 30 min of slow-wave sleep IEEG.